Ocean Engineering 270 (2023) 113656

Contents lists available at ScienceDirect

Ocean Engineering

journal homepage: www.elsevier.com/locate/oceaneng

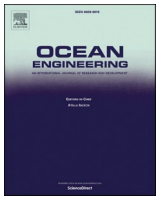

Elucidation of wave pressure acting on a wave-cut notch beneath a coastal cliff based on laboratory experiments and numerical modeling

Masashi Watanabe [a,b,c,*], Taro Arikawa [c]

[a] Earth Observatory of Singapore, Nanyang Technological University, N2-01A-15, 50 Nanyang Avenue, 639798, Singapore
[b] Research and Development Initiative, Chuo University, 1-13-27 Kasuga, Bunkyo-ku, Tokyo, 112-8551, Japan
[c] Faculty of Science and Engineering, Chuo University, 1-13-27 Kasuga, Bunkyo-ku, Tokyo, 112-8551, Japan

ARTICLE INFO

Handling Editor: A.I. Incecik

Keywords:
Coastal cliff
Coastal waves
Coastal boulder
Cliff-top deposition
Impulsive wave pressure
Laboratory experiment

ABSTRACT

To investigate past extreme waves which deposited cliff-top boulders, it is important to elucidate the wave force acting on wave-cut notches beneath coastal cliffs. Our laboratory experiments have revealed that extreme waves over coastal cliffs generated both sustained and impulsive forces, and that sustained forces can be estimated from buoyancy, because velocities are rather small when sustained forces are generated. Thus, boulders at coastal cliffs are likely moved by impulsive forces but not by sustained forces. We have also proposed coefficients of the formula which can reproduce impulsive and sustained wave forces acting on the notch based on observed and simulated wave heights and velocities. Using the proposed formula, wave heights and velocities that are necessary to move boulders up coastal cliffs can be estimated without numerical simulations. In our future investigation, we will account for the scaling effect of impulsive forces acting on coastal cliffs.

1. Introduction

Transport of boulders onto cliff-tops from under cliffs or cliff edges (e.g., Hansom et al., 2008; Watanabe et al., 2019) by tsunami and storm waves has been widely reported around the world (e.g., Autret et al., 2016; Cox et al., 2012; Cox, 2019; Erdmann et al., 2018; Fichaut and Suanez, 2011; Hall et al., 2006, 2008; Hall, 2011; Hansom et al., 2008; Goto et al., 2010, 2011; Kennedy et al., 2017, 2021; Noormets et al., 2004; Pignatelli et al., 2009; Piscitelli et al., 2017; Rovere et al., 2017; Suanez et al., 2009; Williams and Hall, 2004; Watanabe et al., 2019). Most cliff-top boulders have been transported from cliff edges, based on field observation (e.g., Hall et al., 2006, 2008; Hall, 2011; Hansom et al., 2008; Rovere et al., 2017; Williams and Hall, 2004; Watanabe et al., 2019). Cliff-top deposition of coastal boulders has also been investigated in laboratory experiments, which, for example, revealed that a boulder can be transported from a cliff edge (Hansom et al., 2008) and from under a cliff onto the cliff top (Watanabe et al., 2019) by reasonably-sized extreme waves. At cliff topography, it has been found that wave runup is strongly dependent on wave frequency (Carbone et al., 2013), and that a breaking position of a wave is important for boulder movement (Steer et al., 2021).

Other researchers investigated removal of coastal boulders from cliff edges owing to coastal waves (e.g., Kogure et al., 2006; Kogure and Matsukura, 2012; Herterich et al., 2018). Kogure and Matsukura (2012) investigated the relation between the tsunami/storm wave size and the dimensions of boulders which can be removed from coastal cliffs. Herterich et al. (2018) proposed an equation to estimate boulder collapse from cliffs based on the estimation of bending stresses acting on the cliff owing to fluid pressure.

To investigate tsunami or storm wave propagation over cliff-topography, numerical simulation is a powerful, albeit computationally costly, tool. For example, to model wave propagation at coastal cliffs, three-dimensional numerical simulation models or Smoothed Particle Hydrodynamics (SPH) methods (e.g., Rogers and Dalrymple, 2008; Sarfaraz and Pak, 2017) are suitable because they can directly solve pressure acting on the boulder.

The extreme wave force acting on vertical walls or artificial structures such as buildings and piers has been investigated by many studies (e.g., Fukui et al., 1963; Asakura et al., 2000, Arikawa et al., 2005, 2006; Nouri et al., 2010; Carbone et al., 2013; Palermo et al., 2013; Kihara et al., 2015, 2021; Okamoto et al., 2020, 2021; Watanabe et al., 2022), with some studies proposing a formula to estimate wave pressure only from water depth or from water depth and wave velocity (e.g., Arikawa, 2015; Arimitsu and Kawasaki, 2016; Asakura et al., 2000, 2002; Cross,

* Corresponding author. Faculty of Science and Engineering, Chuo University, 1-13-27 Kasuga, Bunkyo-ku, Tokyo, 112-8551, Japan.
E-mail address: masashi.watanabe@ntu.edu.sg (M. Watanabe).

https://doi.org/10.1016/j.oceaneng.2023.113656
Received 18 June 2022; Received in revised form 4 January 2023; Accepted 6 January 2023
Available online 17 January 2023

1967; Sakakiyama, 2012). Some previous studies have investigated wave forces at coastal cliffs (e.g., Hansom et al., 2008; Carbone et al., 2013; Steer et al., 2021), while not proposing a formula to estimate wave force or pressure over coastal cliffs based only on water depth and velocity.

In this study, we have conducted both wave tank experiments and numerical simulations, and proposed a new method to estimate wave pressure/forces over coastal cliffs. For the experiment, a cliff topography was installed in the tank, and solitary waves were generated using a wave maker. The coastal cliff shape was changed multiple times, and each time wave force acting on the cliff was measured. We first revealed the hydraulic characteristics of solitary waves. After that, we conducted numerical simulation of the experiment and validated its accuracy. Based on the results of the experiment and numerical simulation, we then proposed a simple formula to estimate wave pressure without numerical modeling.

2. Method

2.1. Hydraulic experiments

For our experiments, we used a wave tank at Chuo University. The wave tank is 34.08 m long, 0.5 m wide, and 1.0 m high (Fig. 1). The water depth in the wave tank was set to 0.45 m. At $x = 0.0$ m, there is a piston-type wave generator, used to generate soliton waves 5, 10, and 15 cm high (using a scaling of 1:50 based on the Froude similarity law, the waves would have been 2.5, 5.0, 7.5 m high). At $x = 16$–25 m, a slope was set at an angle of 1/20 (Fig. 1). A 20-cm (10-m) high (measured from still water level) vertical wall representing a cliff was set at $x = 25$ m, with a flat topography on top of the cliff (Fig. 1). Extending up to $x = 27$ m. From $x = 30$ m–34.08 m, there is a wave absorber.

We first conducted experiments by inputting soliton waves when a rectangular block was not installed at the cliff edge (Figs. 2 and 3), and then measured time series of water levels and vertical velocities in front of the vertical wall. The time series of water levels were measured at $x =$ 14 m (WG1, water depth; 0.45 m) and $x = 24$ m (WG2, water depth; 0.05 m) with a sampling rate of 100 Hz. The water levels were measured using CHT7-100, which was manufactured by KENEK CO., LTD. The propagation of the soliton waves was recorded at 30 frames per second by a video camera in front of the tank. The bore inundation over the cliff was also recorded using the video camera. Based on the video recording analysis, wave angles (θ), maximum water levels at the cliff, and maximum water levels when the waves reached the cliff (hereinafter, *Hb*) were measured. The definition of these values is shown in Fig. 4.

The above parameters taken from our video analysis were used only to reveal the parameters affecting the magnitude of sustained and impulsive wave forces because of large variance of measurements derived from the video analysis (described in Section 3.1). To propose a new simple formula to estimate wave pressure acting on a coastal cliff only from water level and velocity, we used the simulation results,

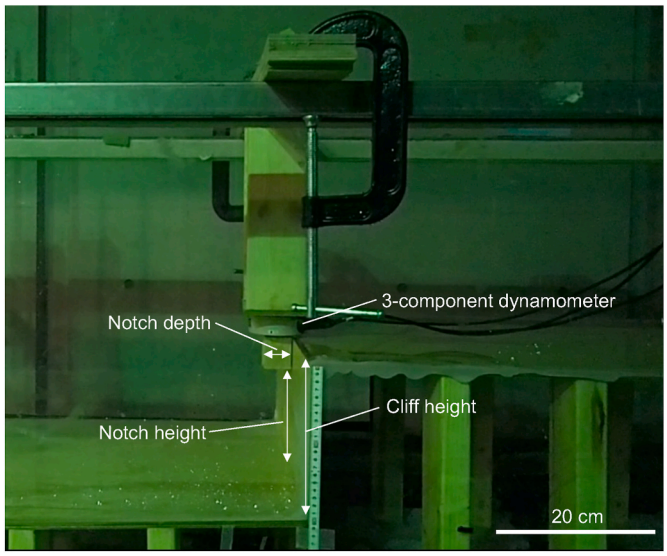

Fig. 2. The laboratory setup in this study. The notch depth, notch height, cliff height, and 3-component dynamometer are indicated.

whose accuracies were validated. When a notch is formed by wave erosion (commonly several meters deep) (Fig. 5), the likelihood of a boulder being transported from a cliff edge by extreme waves increases. This is because when a notch is present, vertical force can act on the bottom of the boulder (e.g., Watanabe et al., 2019). To reproduce a cliff notch in the experiment, we installed a rectangular block at the cliff edge (a gap was left between the block and the vertical wall representing the cliff to prevent friction, but it was tiny enough to prevent water from entering the gap), and measured vertical and horizontal wave force acting on the notch with a 3-component dynamometer fixed at the rectangular block (Figs. 1 and 2). The forces acting on the rectangular block were measured using LSM-B-100NSA1Z10-P, which was manufactured by Kyowa Electronic Instruments CO., LTD.

When a tsunami is close to the shore, a bore is generated owing to wave breaking and soliton fission at the leading edge of the tsunami. The maximum value of force generated when the bore impacts an object is called impulsive force (Arikawa et al., 2005). After that, continuous arrival of tsunami waves raises the water level. The force which is generated during this phase is called sustained force (Arikawa et al., 2005). Examples of both impulsive and sustained force are shown in Fig. 6. For measuring wave pressure when impulsive wave force is generated, it is recommended that sampling rate should be set as more than 1000 Hz (Shimosako, 2001). We set the sampling rate of the dynamometer at 1000 Hz. The resultant impulsive wave is described in Section 3.1. Owing to the shape of the coastal cliff, the wave force acting on the notch changes. In this study, we varied the height and depth of rectangular blocks (hereinafter the notch height and notch depth,

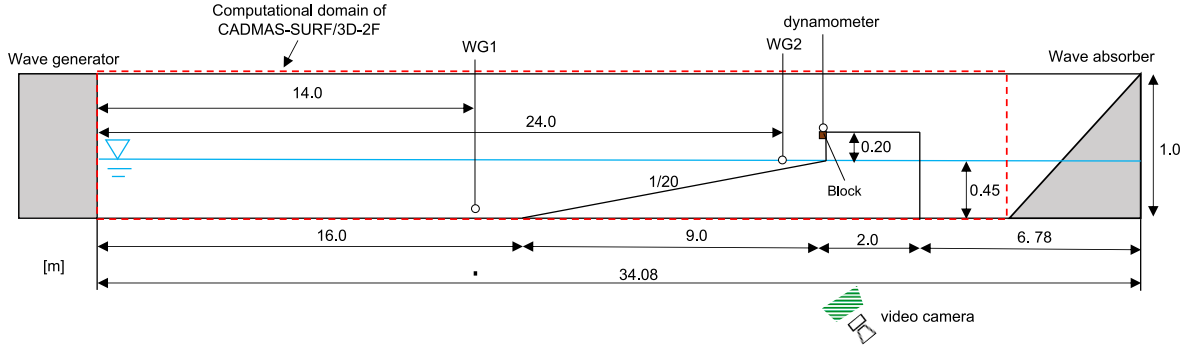

Fig. 1. A schematic diagram of the wave tank. The numerical domain for the CADMAS-SURF/3D-2F is also shown.

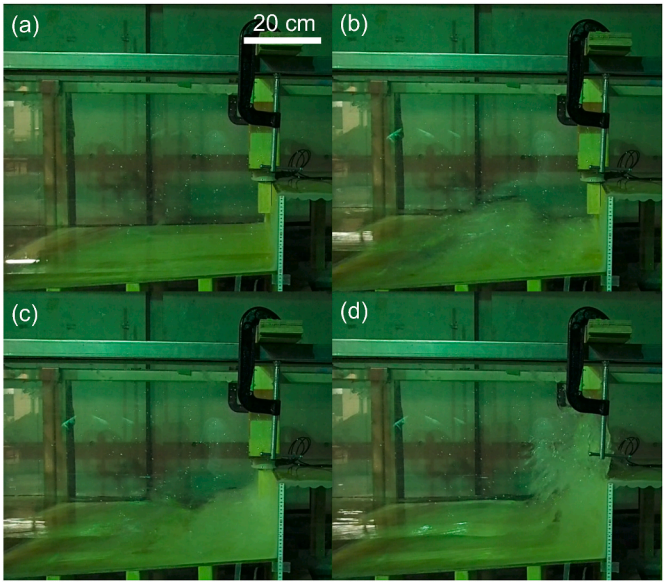

Fig. 3. Laboratory video stills for wave height of 10 cm, notch depth of 4 cm, and notch height of 10 cm. (a) Before the experiment (0 s after the wave generation); (b) when the wave reached the vertical cliff (36.64 s after the wave generation); (c) when the wave reached the notch (36.8 s after the wave generation); (d) when the wave reached the maximum water level (37.04 s after the wave generation).

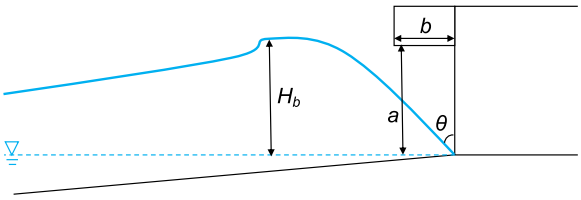

Fig. 4. The definition of symbols and a conceptual diagram of the notch at the coastal cliff used in this study. H_b is the maximum water level when the generated wave reached the cliff, θ is the wave angle, a is the notch height, and b is the notch depth.

Table 1) installed at the cliff edge to reveal the wave force of coastal waves at various types of coastal cliffs. We set the notch height as 5, 10, and 15 cm and the notch depth as 2, 4, and 6 cm. The width of the block remained constant at 3.5 cm. All experiments were repeated three times for each case to account for variability. In all cases, both impulsive forces and sustained forces were generated, although, in some cases, sustained forces and impulsive forces could not be separated. We excluded such data from our experimental data summary and from comparison of observed and simulated values.

2.2. Numerical simulations

We conducted three-dimensional simulations of the laboratory experiments using CADMAS-SURF/3D-2F, which is three-dimensional incompressible viscous fluid, and Navier–Stokes equations (Fig. 7) to propose a simple formula to estimate wave pressure acting on coastal cliffs only from water level and velocity.

2.2.1. CADMAS-SURF/3D-2F

CADMAS-SURF/3D-2F (Arikawa et al., 2005) is a numerical wave-tank flume model developed for advanced maritime structure design. This model comprises Equations (1)–(4). equation (1) is continuous for the three-dimensional incompressible viscous fluid and equations (2)–(4) are Navier–Stokes equations in the x, y, and z directions developed based on the volume of the porous model.

$$\frac{\partial \gamma_x u}{\partial x}+\frac{\partial \gamma_y v}{\partial y}+\frac{\partial \gamma_z w}{\partial z}=\gamma_v S_\rho \tag{1}$$

$$\lambda_v\frac{\partial u}{\partial t}+\frac{\partial \lambda_x uu}{\partial x}+\frac{\partial \lambda_y vu}{\partial y}+\frac{\partial \lambda_z wu}{\partial z}=-\frac{\gamma_v}{\rho}\frac{\partial p}{\partial x}+\frac{\partial}{\partial x}\left\{\gamma_x \nu_e\left(2\frac{\partial u}{\partial x}\right)\right\}$$
$$+\frac{\partial}{\partial y}\left\{\gamma_y \nu_e\left(\frac{\partial u}{\partial y}+\frac{\partial v}{\partial x}\right)\right\}+\frac{\partial}{\partial z}\left\{\gamma_z \nu_e\left(\frac{\partial u}{\partial z}+\frac{\partial w}{\partial x}\right)\right\}-\gamma_v D_x u-R_x+\gamma_v S_u \tag{2}$$

$$\lambda_v\frac{\partial v}{\partial t}+\frac{\partial \lambda_x uv}{\partial x}+\frac{\partial \lambda_y vv}{\partial y}+\frac{\partial \lambda_z wv}{\partial z}=-\frac{\gamma_v}{\rho}\frac{\partial p}{\partial y}+\frac{\partial}{\partial x}\left\{\gamma_x \nu_e\left(\frac{\partial v}{\partial x}+\frac{\partial u}{\partial y}\right)\right\}$$
$$+\frac{\partial}{\partial y}\left\{\gamma_y \nu_e\left(2\frac{\partial v}{\partial y}\right)\right\}+\frac{\partial}{\partial z}\left\{\gamma_z \nu_e\left(\frac{\partial v}{\partial z}+\frac{\partial w}{\partial y}\right)\right\}-\gamma_v D_y v-R_y+\gamma_v S_v \tag{3}$$

$$\lambda_v\frac{\partial w}{\partial t}+\frac{\partial \lambda_x uw}{\partial x}+\frac{\partial \lambda_y vw}{\partial y}+\frac{\partial \lambda_z ww}{\partial z}=-\frac{\gamma_v}{\rho}\frac{\partial p}{\partial y}+\frac{\partial}{\partial x}\left\{\gamma_x \nu_e\left(\frac{\partial w}{\partial x}+\frac{\partial u}{\partial z}\right)\right\}$$
$$+\frac{\partial}{\partial y}\left\{\gamma_y \nu_e\left(\frac{\partial w}{\partial y}+\frac{\partial v}{\partial z}\right)\right\}+\frac{\partial}{\partial z}\left\{\gamma_z \nu_e\left(2\frac{\partial w}{\partial z}\right)\right\}-\gamma_v D_z w-R_z+\gamma_v S_w+\frac{\gamma_v \rho^* g}{\rho} \tag{4}$$

where, t stands for time, x and y are the horizontal coordinates, and z is the vertical coordinate. Also, u, v, and w, respectively, represent the flow velocity components in the x, y, and z-directions. p stands for pressure, ρ is the reference density, ρ^* represents buoyancy considering the density, ν denotes viscosity, ν_t stands for eddy viscosity, ν_e expresses the sum of the molecular kinematic ν and ν_t, and g signifies the acceleration of gravity. γ_x, γ_y, and γ_z, respectively, represent the area transmittance in the x, y, and z directions. λ_x, λ_y, and λ_z are inertia coefficients. D_x, D_y, and D_z are coefficients for the energy damping area. R_x, R_y, and R_z are drag forces from the porous model. S_ρ, S_u, S_v, and S_w are source terms for the wave-making source.

2.2.2. Conditions of numerical simulations

For the simulations using CADMAS-SURF/3D-2F, we adopted a nonuniform grid-cell (0.05–0.005 m) in the vertical grid cell. The sizes in x, y, and z directions in the computational domain were set as 34 m, 0.5 m, and 1.0 m, respectively. The grid cell size in the x and y directions was 0.02 m. The grid cell size in the z direction was 0.05–0.005 m. We used fine grid-cells near the water surface and coarse ones for the other areas. The time-cell size was determined automatically based on the Courant number. The simulation time was 25 s. In the numerical domain, the upper area was defined as the free boundary, while the remaining areas were defined as slip boundary. At the far downstream position of $x = 30$ m, a damping area was set to absorb incoming waves. The VOF (Volume of Fluid) method (Hirt and Nichols, 1981) was applied to calculate the free surface of the water.

A soliton wave was input in the numerical domain using the following equation:

$$\eta(x,t)=H\,\mathrm{sech}^2\left(\sqrt{\frac{3H}{4h^3}}\left(x-\sqrt{g(h+H)}\,t\right)\right) \tag{5}$$

where, $\eta(x,t)$ is the water level, H is the wave height, h is the distance from the bed to the water surface. The soliton wave heights were 0.05 m, 0.1 m, and 0.15 m (Table 1) at the water depth of 0.45 m.

For the simulations, the vertical force acting on the notch was calculated by integrating the simulated pressure over the projected area of the notch bottom. We conducted parallel computing using an Earth simulator (ES4), which is a multi-architecture supercomputer owned by Japan Agency for Marine-Earth Science and Technology (JAMSTEC) (JAMSTEC, undated), with the total peak performance and total memory, respectively, of 19.5 PFLOPS and 556.5 TiB. In this study, we used

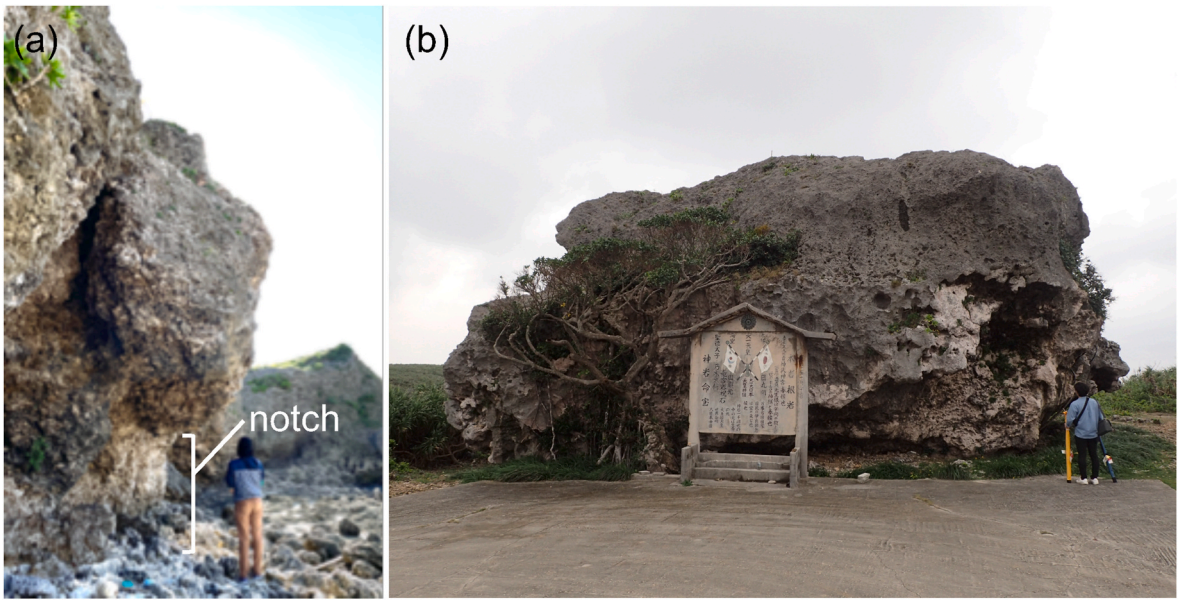

Fig. 5. The photographs of (a) notch formed under the cliff on Shimoji Island, Japan and (b) boulder located at the cliff-top in the same location. The weight of the boulder is approximately 6000 tons (Goto et al., 2010).

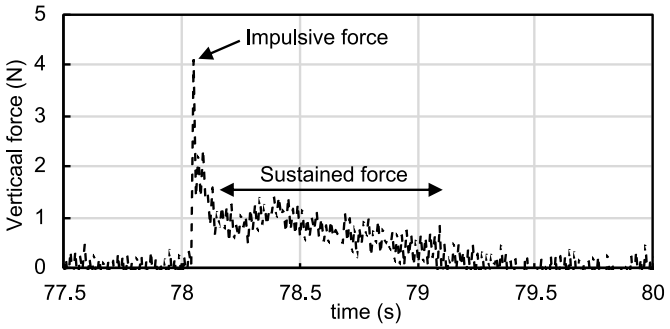

Fig. 6. An example of impulsive force and sustained force when the generated wave height was 10 cm, notch height was 10 cm, and notch depth was 4 cm.

Table 1
Experimental conditions.

Water depth (m)	0.45
input wave height (m)	0.05, 0.1, 0.15
notch depth (m)	0.02, 0.04, 0.06
notch height (m)	0.05, 0.1, 0.15

684 VE-equipped Nodes of the Earth Simulator (ES4). In the VE-equipped Nodes, the total memory of the host part is 128GiB, and the total memory of the accelerator is 48GiB (JAMSTEC, undated).

2.3. Estimation of wave pressure without numerical modeling

Methods to estimate pressure acting on the notch not using numerical simulations have also been widely used. In general, pressure can be determined from the inundation depth d (e.g., Arikawa, 2015; Arimitsu and Kawasaki, 2016; Asakura et al., 2000, 2002; Sakakiyama, 2012) or the inundation depth d and flow velocity u (e.g., Cross, 1967; Arimitsu and Kawasaki, 2016; Kihara et al., 2021). Equations to express wave pressure are sometimes expressed by the sum of the hydrostatic and hydrodynamic pressure, which is how the pressure over the notch was estimated in this study. The equation is as follows:

$$P_{max} = \rho g(\alpha_d h - Z) + \frac{1}{2}\rho C_P u^2 \text{ for } 0 \le Z \le \alpha_d h, \text{ and}$$

$$p = 0 \text{ for } Z > \alpha_d h \tag{6}$$

where, P_{max} is the maximum pressure on the buildings, g is the acceleration of gravity, Z is the distance from the bed, h is the distance from the bed to the water surface, and α_d is a coefficient of no dimensional wave pressure (Asakura et al., 2000), u is the typical speed, C_P is the pressure coefficient. In the typical speed, we used the vertical velocity in front of the cliff when the block was not installed. The velocities in front of the vertical cliff at the time that maximum vertical impulsive and sustained forces were measured were defined as the typical speed in this study. For the water level for the calculation of P_{max}, we also used the values at the time that both types of force were measured when the block was not set at the cliff edge. For the distance from the bed ($= Z$), we used the value of notch height. We used the measured maximum impulsive and sustained pressure as P_{max}. For the water level and typical velocity for the calculation of P_{max}, we used the calculation values from CADMAS-SURF/3D-2F. As mentioned in section 3.2 below, the measured time series of water level and pressure acting on the notch were reasonably reproduced. The above equations were proposed to reveal the tsunami wave pressure on a sea wall or structure (e.g., Asakura et al., 2002). In this study, we estimated the coefficients α_d and C_P, which can estimate impulsive and sustained pressure over the notch at coastal cliffs.

Firstly, we varied the values of α_d between 1.0 and 3.0 at 0.01 increments and $C_P = 0.0$ to investigate whether the pressure over the notch can be expressed without hydrodynamic pressure. Secondly, we varied C_P within the range of 1.0–3.0 at 0.01 increments while $\alpha_d = 1.0$ to determine the C_P value that represents hydrodynamic pressure.

To determine the values of α_d and C_P that can explain the observed pressure, we used the geometric mean K and the log-normal standard deviation κ. The definitions of these values are as follows:

$$log(K) = \frac{1}{n}\sum_{i=1}^{n} ln\left(\frac{Obs}{Cal}\right) \tag{7}$$

$$log(\kappa) = \left[\frac{1}{n}\left\{\sum_{i=1}^{n}\left(log\left(\frac{Obs}{Cal}\right)\right)^2 - n(ln\,K)^2\right\}\right]^{1/2} \tag{8}$$

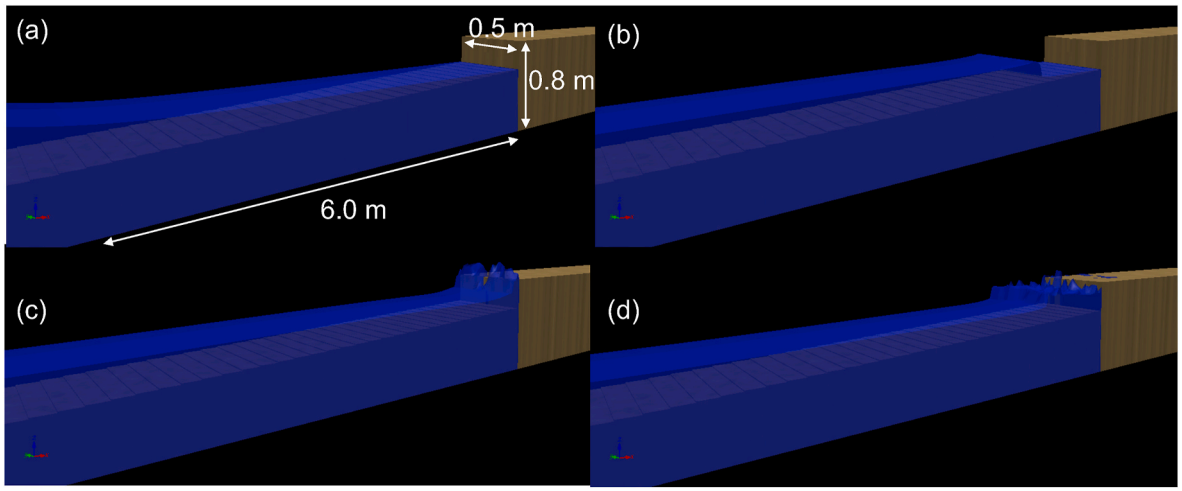

Fig. 7. Snapshots of numerical simulations with the CADMAS-SURF/3D-2F when the generated wave height was 10 cm, notch depth was 4 cm, and notch height was 10 cm. The snapshots are at (a) 13.45 s, (b) 15.0 s, (c) 15.6 s, and (d) 16.2 s after the start of the simulation.

where, *Cal* and *Obs* denote the predicted and measured values at the measurement point, respectively, and n is the number of points comparing the physical quantity. K and κ (Aida, 1978) indicate the geometric average value and the fluctuation in the ratio of the observed to computed values, respectively. A high value of K means a high difference between the calculated and observed results. Similarly, a high value of κ means a high variability of the calculated and observed results. The K and κ have been used to validate estimation methods of wave pressure by quantitatively comparing estimated and observed values (e.g., Kihara et al., 2021; Watanabe et al., 2022). We also output the relation between the Froude number ($F_r = u/\sqrt{gd}$) and impact/-sustained forces. For the Froude number, g is the acceleration of gravity, and u and d are the flow velocity and inundation depth of the flow, respectively. The velocity u was assumed to be at the bottom of the notch, while the inundation depth d was assumed as the water depth when maximum impact/sustained pressures were measured. These two values were also simulated using CADMAS-SURF/3D-2F.

To include the component of hydrodynamic pressure, some studies proposed a method to estimate the value of α_d based on the value of F_r (e.g., Arikawa, 2015; Arimitsu and Kawasaki, 2016; Asakura et al., 2002; Kato et al., 2012; Sakakiyama, 2012). For example, Kato et al. (2012) proposed the following relation which is determined by the Froude number:

$$\alpha_d = 1.0 + 0.5F_r^2 \quad (C_P = 0.0) \tag{9}$$

where, $F_r(= u/\sqrt{gd})$ is the Froude number, g is the acceleration of gravity, and u and d are the velocity and inundation depth of the flow, respectively. To calculate F_r for the case when the rectangular block was not installed at the cliff edge, we used values for the vertical velocity at the bottom of the notch and for the water depth when maximum sustained forces were observed. Impulsive wave forces were observed when the waves reached the bottom of the notch, thus water level from the bottom of the notch was almost zero. Thus, if the relation of equations (6) and (9) are used, impulsive wave forces were zero. Therefore, we applied this method only for sustained forces.

3. Results

3.1. Hydraulic experiment

A soliton wave generated by the wave maker propagated on the slope, reaching the vertical wall (cliff), where the water rushed vertically up, and often over, the wall (Fig. 3). The time series of water levels is shown in Fig. 8. When the input wave height was 5 cm, the maximum water level at the vertical wall was 16 cm, and the bore did not reach the clifftop. With 10 cm and 15 cm initial wave heights, the maximum water level in front of the vertical wall was, respectively, 32 cm and 37 cm (Table 2). In these cases, the wave reached to the cliff-top and inundated the land behind it.

The maximum measured horizontal and vertical forces were, respectively, 2.56 N and 11.8 N (Fig. 9). The time series of measured vertical wave forces when the input wave height was 10 cm, notch heights were 5 cm, 10 cm, and 15 cm, and the notch depth was 4.0 cm are shown in Fig. 10. Impulsive forces were initially observed, with the duration of less than 0.1 s in all cases, when the leading edge of the input wave reached the notch. Also, maximum impulsive forces observed corresponded with increases in the Froude number. After the observation of impulsive forces, water level reached maximum values, and at the same time vertical velocity and the Froude number decreased. After that, the maximum sustained wave force was generated (Fig. 10). The observed impulsive wave forces were 11.8–1.23 N, and the observed sustained wave forces were 3.35–0.77 N (Fig. 9).

The relationship between the wave angle, maximum water level at the cliff, and *Hb* versus maximum vertical impulsive and sustained forces were derived (Fig. 11 a-f). The measured ranges of all parameters in Fig. 11 increased when both impulsive and sustained forces increased. The input wave height, notch height, and notch depth versus maximum vertical impulsive and sustained forces are also shown (Fig. 12). There are negative correlations between wave angle and impulsive force as well as wave angle and sustained force (Fig. 11a and d). If size of input wave increases, water level in front of the cliff increases. Then, the vertical impulsive and sustained forces increase. Thus, there is a positive correlation between the maximum water level at the cliff and input wave height and impulsive and sustained force (Fig. 11b, e, 12). Vertical force increases with the increase in the notch depth (Fig. 9). This is because the projected area of vertical force increases. When the bottom of the notch is close to the still water level, the pressure acting on the notch bottom increases with increasing water depth as measured from the bottom of the notch (Fig. 9).

3.2. Numerical simulation

Firstly, we compared simulated water levels and water levels observed at water gauges WG1 and WG2 (Fig. 8). The computed time series of water levels at 17.5–18.5 s for a 5-cm wave height and at 15.5–17 s for a 10-cm wave height are underestimated in the calculation. This is because the movement of the wave generator piston is not

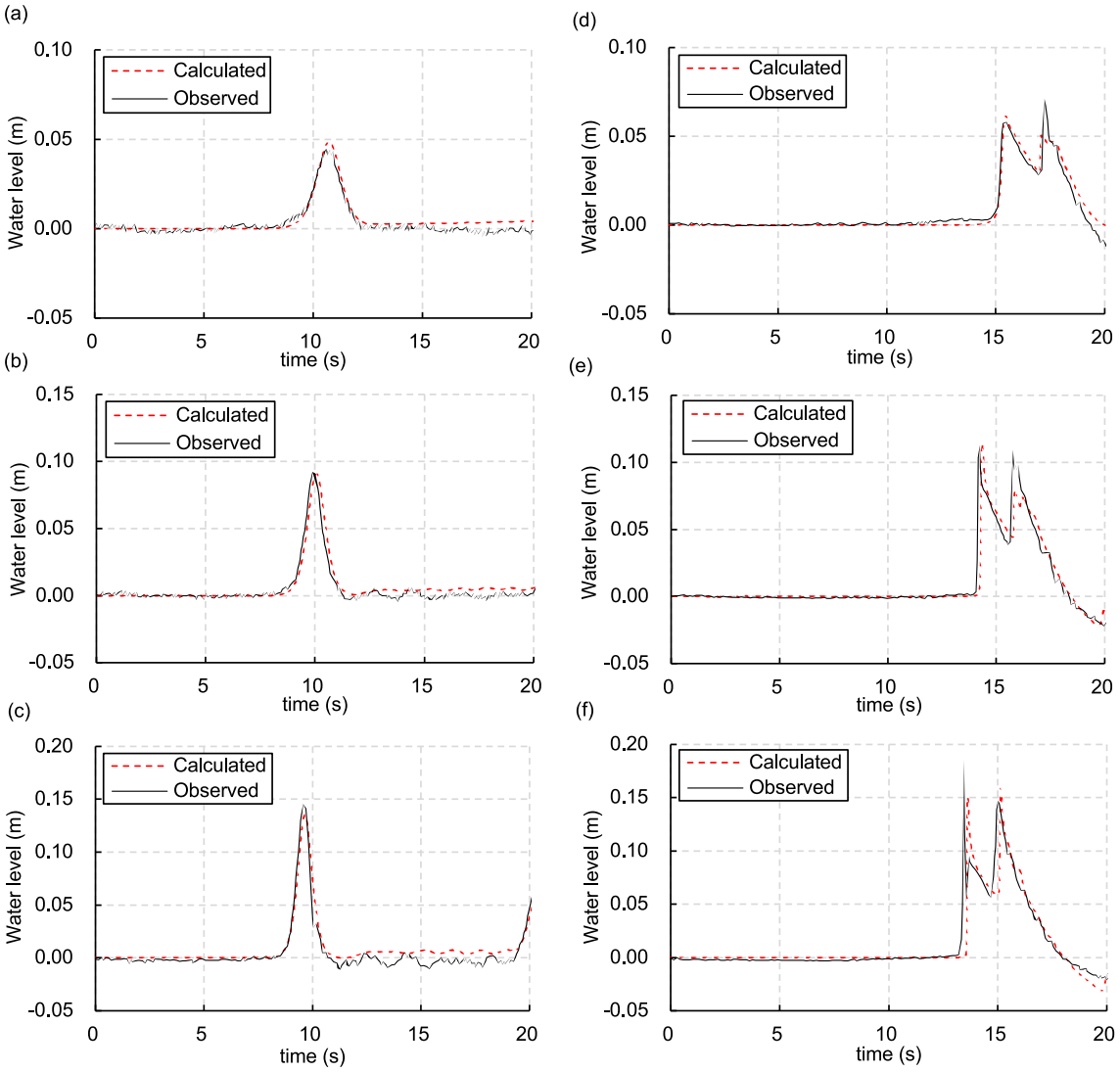

Fig. 8. Time series of water levels measured during the experiment and simulated by the CADMAS-SURF/3D-2F at WG1 when the generated wave height was (a) 5 cm, (b) 10 cm, and (c) 15 cm. Time series of water levels measured during the experiment and simulated by the CADMAS-SURF/3D-2F at WG2 when input wave height was (d) 5 cm, (e) 10 cm, and (f) 15 cm.

Table 2
The wave height of generated soliton waves, observed maximum water levels in front of the cliff, offshore maximum water levels, and wave angles.

Wave height (cm)	5	10	15
Maximum water level in front of cliff (m)	0.16	0.32	0.37
Offshore maximum water level (m)	0.066	0.17	0.15
Wave angle (°)	62.3	58.2	53.3

reproduced in the simulation. Another reason is that the shapes of the dynamometer and the instruments supporting the dynamometer are not included in the simulation. In this study, we concentrated on maximum impulsive and sustained pressure generated during the first wave. As shown in Fig. 8, the computed water levels of first waves is consistent with the observed values (Fig. 8).

We also compared the simulated and observed vertical impulsive and sustained forces acting on the notch (Fig. 12). The simulated maximum sustained forces were reasonably consistent with observed maximum sustained forces. Also, the simulated maximum impulsive forces were reasonably consistent with observed maximum impulsive forces. However, the accuracy of numerical modeling of maximum impulsive forces was lower than the accuracy of numerical modeling of sustained forces (Fig. 12). The same accuracy issue was encountered by Arikawa et al. (2021) during numerical simulation of wave pressure acting on vertical cliffs. The issue arises because simulations of impulsive forces need to account for air that is compressed between the wave and the cliff as well as for air pockets inside the wave. The relationship between pressure and notch height, notch depth, and input wave height was reproduced reasonably accurately. The observed time series of vertical forces were also reasonably consistent with the simulated values (Fig. 10).

The maximum impulsive and sustained wave forces versus the Froude number are shown in Fig. 13. When the maximum impulsive wave forces were generated, the Froude numbers were between 1.41 and 2.91. When the maximum sustained wave forces were generated, the Froude numbers were between 0.16 and 0.32. In the case of impulsive wave forces, the forces increased with the increase in the Froude numbers (Fig. 13). The distributions of velocities and pressures over the cliff are shown in Figs. 14 and 15, respectively. Observation points of the maximum wave velocities and pressures on CADMAS-SURF/3D-2F were set at 0.5-cm intervals on the cliff when the notch was not installed (Figs. 14a and 15a) and when it was installed (Fig. 15b). In the area of <2.5 cm from the still water level, horizontal

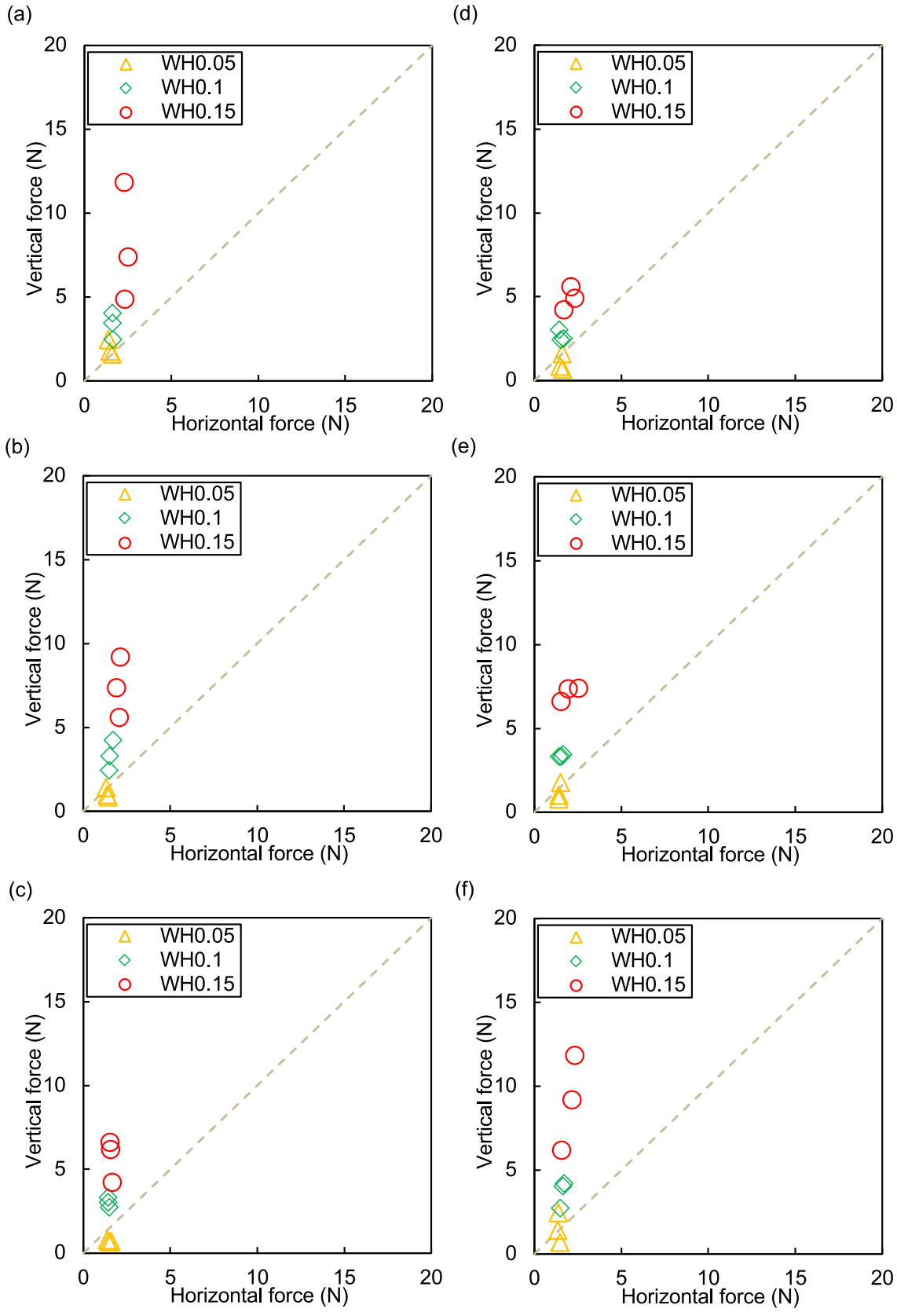

Fig. 9. The observed vertical and horizontal wave forces and wave forces on the coastal cliff. In the symbols, WH presents value of input wave height (m). The vertical and horizontal forces when notch height is (a) 5 cm, (b) 10 cm, and (c) 15 cm and notch depth is (d) 2 cm, (e) 4 cm, and (f) 6 cm are shown.

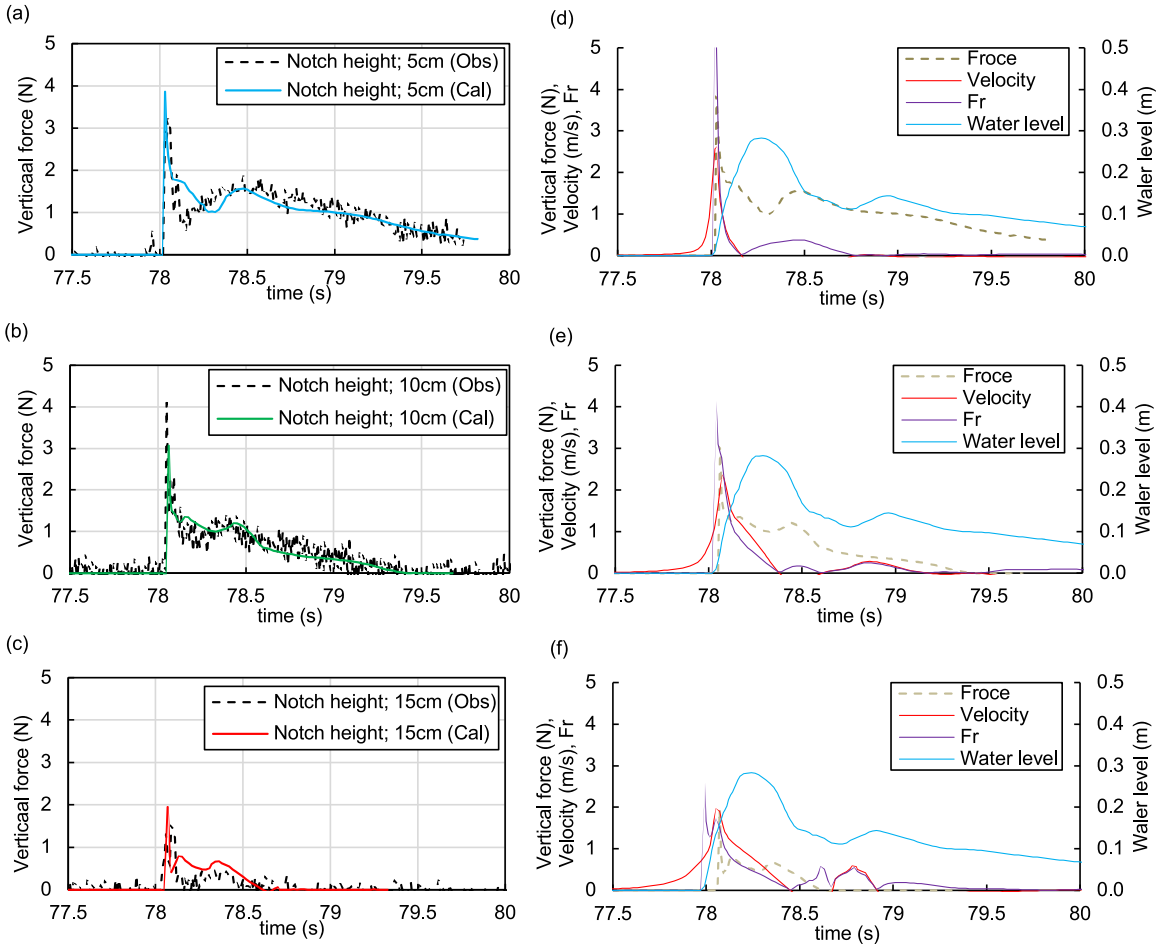

Fig. 10. Time series of vertical force measured during the experiment and simulated by the CADMAS-SURF/3D-2F when the generated wave height was 10 cm, notch depth was 4 cm, and notch height was (a) 5 cm, (b) 10 cm, and (c) 15 cm. The time series of vertical wave force, water level, vertical velocity, and the Froude number (F_r) simulated by the CADMAS-SURF/3D-2F. The water level was simulated in front of the vertical cliff when a rectangular block was not installed at the cliff edge.

velocities are higher than vertical velocities, meaning that vertical wave forces become significant within the area of 2.5–20 cm from the still water level (Fig. 14c). At the vertical wall, within the area of 2.0–4.0 cm from the still water level, wave pressure increased in all cases because the waves hit this cliff area first (Fig. 15). In the cases of all notch heights, the pressure also increased in the area where the notch was installed. In all other areas, the values of computed pressure were almost identical with the values calculated when the notch was not installed (Fig. 15).

The comparison of observed maximum Impulsive and sustained pressure and estimated pressure using equation (6) are shown in Fig. 16. When hydrostatic pressure was used ($C_P = 0.0$, $\alpha_d = 1.0$), the observed sustained pressure was consistent with the calculated values (Fig. 16a), and the values of K and κ were, respectively, 1.06 and 0.76 (Table 3). When hydrodynamic pressure was not assumed ($C_P = 0.0$), the K values were mostly small when $\alpha_d = 1.0$ (Table 3). For the impulsive pressure, K and κ were 0.015 and 3.0, respectively, when hydrostatic pressure was used ($C_P = 0.0$, $\alpha_d = 1.0$) (Table 3). In this case, most calculated (using equation (6)) pressures were underestimated (Fig. 16b).

In the case when hydrodynamic pressure was assumed, the K values for impulsive pressure were mostly small when $C_P = 1.38$ and $\alpha_d = 1.0$ (Fig. 16d). In these cases, K and κ were, respectively, 1.0 and 1.31 (Table 3). When $C_P = 1.38$ and $\alpha_d = 1.0$, K and κ of sustained pressures were, respectively, 1.14 and 0.79. When $C_P = 1.38$ and $\alpha_d = 1.0$ were assumed for sustained pressures, estimated pressures were consistent with the observed values (Fig. 16c).

When equation (9) was used, the sustained forces were also reproduced reasonably accurately (Fig. 16e). In this case, K and κ were, respectively, 1.17 and 0.72 (Table 3). This is because the Froude number is small during sustained forces (Fig. 13), thus α_d is close to 1.0 when equation (9) is used.

4. Discussion

4.1. Wave force acting on the coastal cliff

In the experiment, both impulsive and sustained forces were observed as in the case of tsunami load on vertical walls (e.g., Fukui et al., 1963; Asakura et al., 2000, Arikawa et al., 2005, 2006, Nouri et al., 2010; Palermo et al., 2013; Kihara et al., 2015). Impulsive force, which was stronger than sustained force (Fig. 13), increased with the decrease in wave angles and increase in the maximum water level at the cliff (Fig. 11). Sustained force was reproduced when (α_d, C_P) = (1.0, 0.0) (Fig. 16), meaning that sustained force can be expressed as hydrostatic pressure/buoyancy. Thus, sustained force cannot move a boulder whose density is higher than water upward, and the boulder is moved by impulsive forces.

The influence of impulsive force on boulder transport was also investigated by Nandasena and Tanaka (2013), who revealed that impact force contributes to initial velocity of a rectangular block over the shoreline owing to dambreak flow. They then revealed that impulsive force does not contribute to time series of boulder velocity and

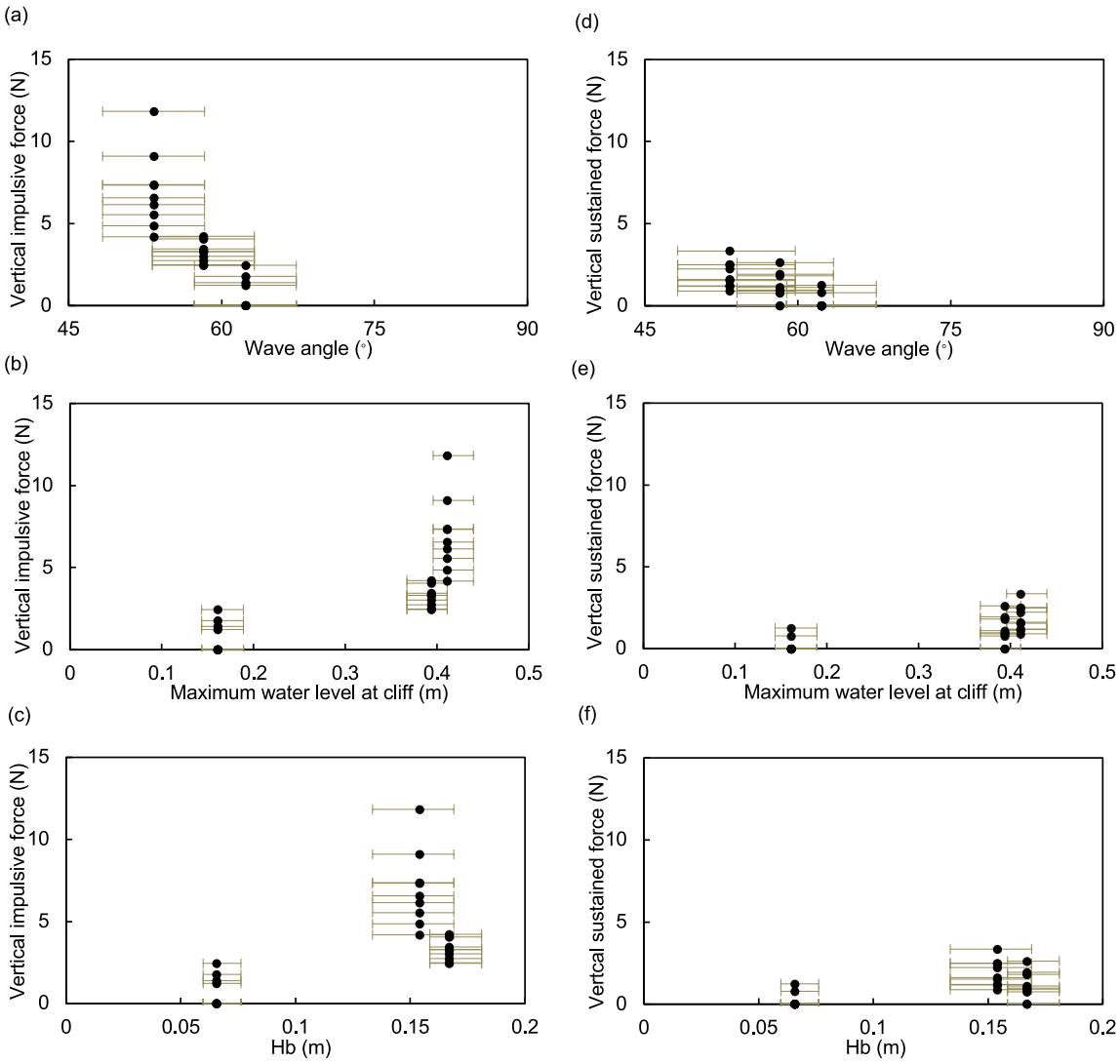

Fig. 11. The observed impulsive vertical wave forces acting on the coastal cliff versus (a) wave angle, (b) maximum water level at the cliff, (c) maximum water level when the wave reached the cliff (H_b). Also shown are the observed sustained vertical wave forces acting on the coastal cliff versus (d) wave angle, (e) maximum water level at cliff, (f) H_b. In these figures, we showed measured range of the experiments.

boulder transport distance after a wave hits a boulder.

To estimate the minimum wave height to move a boulder, Nott's (2003) model has been widely used (e.g., Whelan and Kelletat, 2005; Mastronuzzi et al., 2007; Spiske et al., 2008; Costa et al., 2011; Miller et al., 2014; Gandhi et al., 2017). Nott's model assumes the Froude numbers of tsunami as 2. In our experiment, the Froude numbers for impulsive waves were 1.41–2.91, which is a comparable range to Nott's model, and 0.10–0.40 for sustained forces (Fig. 13), which is much smaller that the Froude number in Nott's model. Thus, the minimum wave height to move a coastal cliff boulder by sustained forces cannot be reasonably estimated using Nott's model. The Froude number proposed by Nott (2003) is 2.0 and our experimental results in the case of impulsive waves are within the range of this value (Fig. 13). Thus, the initiation of boulder transport from the cliff edge by impulsive forces of tsunami waves can be calculated using Nott's equation.

4.2. The formulation which can estimate wave force acting on the coastal cliff

Kihara et al. (2021) investigated the coefficients of α_d and C_P to reproduce tsunami wave force acting on the structure. For the case that impulsive force was generated, they found that (α_d, C_P) = (1.0, 1.5) reproduced tsunami wave force on the structure best. In our experiment, the parameters which best reproduced vertical impulsive wave (α_d, C_P) = (1.0, 1.38) were close to Kihara et al.'s values. This is because in both experiments, high hydrodynamic forces were generated. However, when the coefficient of hydrodynamic component is not included, such as when (α_d, C_P) = (3.0, 0.0) were assumed (parameters in Asakura et al., 2002), the K value was 0.022, which means that the estimated force was lower than the observed force.

Our values of (α_d, C_P) = (1.0, 1.38) or equation (9) can also be used to reproduce sustained wave force acting on the notch (Fig. 16c and e) because the velocity and hydrodynamic force when sustained force was generated were quite small. Thus, sustained pressure can be reproduced without considering hydrodynamic components. Therefore, the values (α_d, C_P) = (1.0, 1.38) can be used for both impulsive forces and sustained forces. The κ value when (α_d, C_P) were used to estimate impulsive wave pressure was further from 1.0 than the κ value when (α_d, C_P) were used to estimate sustained wave pressure (Table 3). This is because the variability of measurement of impulsive wave forces is higher than that of sustained forces.

In this study, we confirmed that our proposed formula can estimate impulsive and sustained wave forces acting on the notch. When this proposed simple method is combined with the method of Herterich et al.

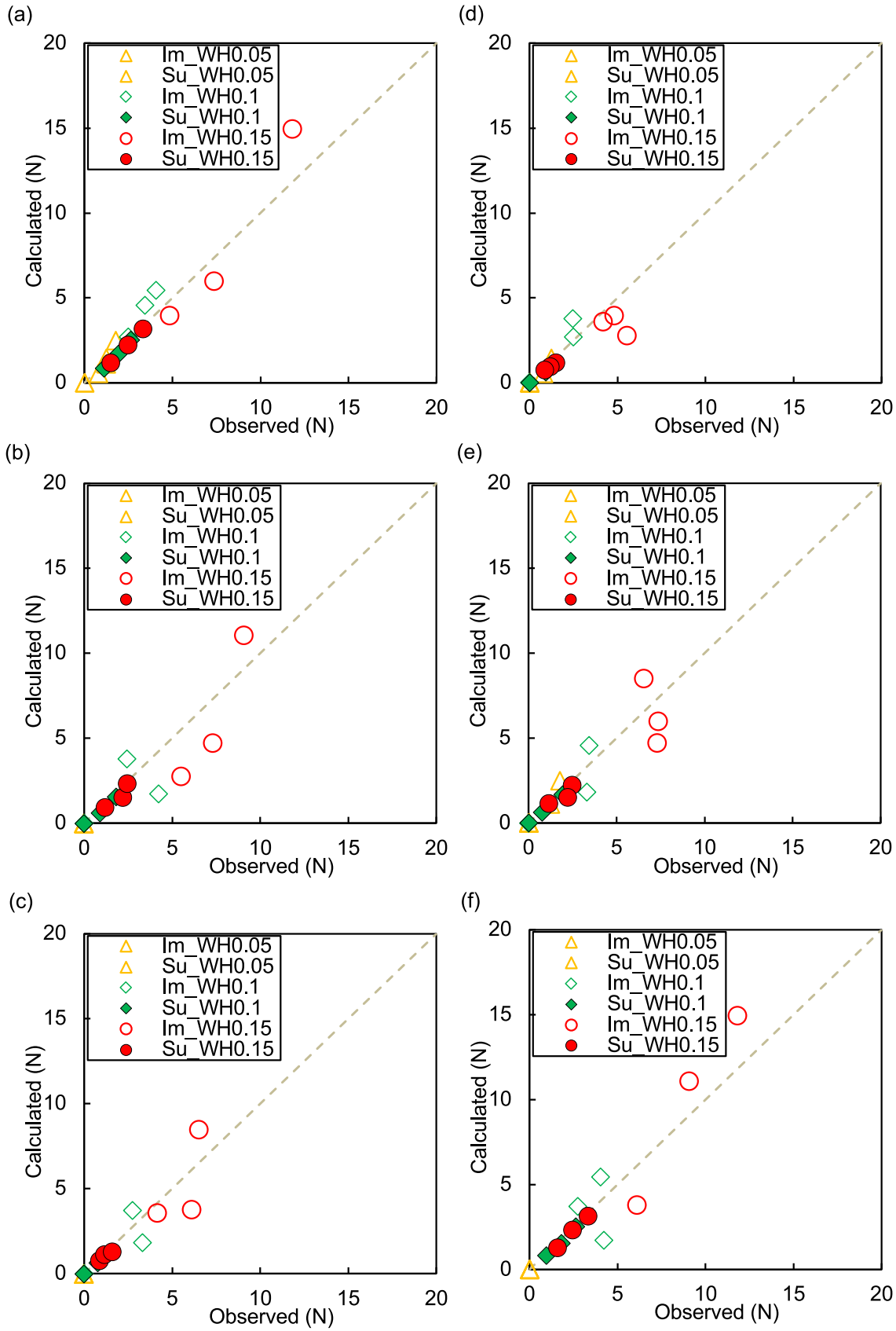

Fig. 12. The observed impulsive and sustained vertical wave forces and wave forces simulated by the CADMAS-SURF/3D-2F acting on the coastal cliff. In the symbols, Im and Su present the values of impulsive and sustained forces, respectively. WH presents value of input wave height (m). The simulated and observed forces when notch height is (a) 5 cm, (b) 10 cm, and (c) 15 cm and notch depth is (d) 2 cm, (e) 4 cm, and (f) 6 cm are shown.

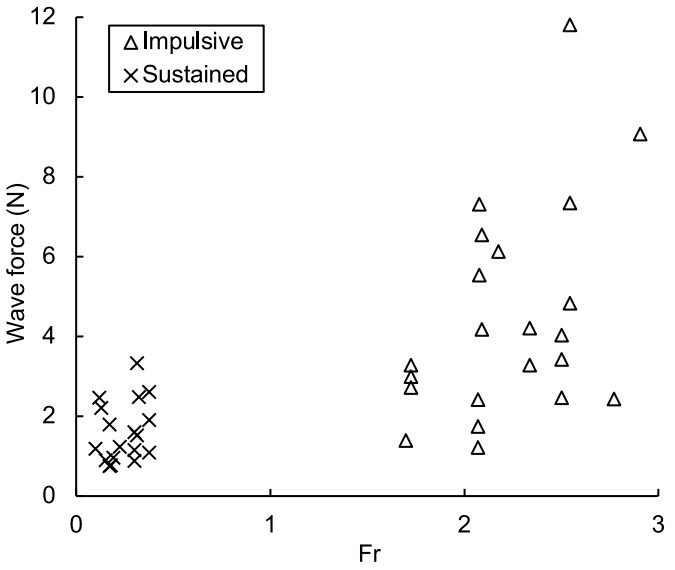

Fig. 13. The observed maximum impulsive and sustained wave forces versus the Froude number.

(2018) for calculating bending stress, we can also estimate the water depth and velocity that are necessary to remove (break off) the boulder from the cliff's edge. In the experiment, we used Froude scaling. While Froude scaling cannot not scale viscous forces, capillary forces, and air compressibility reasonably accurately, viscous forces have only local effect in the cliff topography, and capillary forces are negligible for waves at both full and model scales (Hansom et al., 2008). In comparison, air compressibility–when a large wave impact traps air between the cliff and the wave–is important for wave force measurement (Hansom et al., 2008) and can significantly affect impulsive wave force measurement at experimental levels (Kihara et al., 2015). However, air compressibility cannot be scaled (Shimosako et al., 2001). Future studies should aim at investigating impulsive forces over coastal cliffs at lower scales.

5. Conclusion

While coastal boulders transported from cliff edges or from under cliffs have frequently been observed, the characteristics of wave forces acting on the notch at the cliff topography have not been investigated.

Firstly, we conducted laboratory experiments to measure wave forces acting on a coastal cliff. We have revealed that vertical force (maximum observed value of 11.8 N) is high compared to horizontal force (maximum observed value of 2.34 N). Both impulsive and sustained wave forces were observed, just as in the case of tsunami load at vertical structures. We have confirmed that the magnitude of the observed vertical force increases when the notch height is low, notch depth is long, and the maximum water depth at the cliff is high.

Secondly, we conducted numerical simulation using the three-dimensional simulation model CADMAS-SURF/3D-2F. The time series of vertical wave force acting on the notch was reasonably reproduced, with the accuracy of numerical simulation of impulsive forces being lower than the accuracy of numerical simulation of sustained forces. The Froude numbers for impulsive waves were 1.41–2.91 and 0.16–0.32 for sustained forces.

Thirdly, after the validation of the numerical simulation, we have proposed the values of α_d and C_P that can reproduce impulsive and sustained wave pressure acting on the notch. When $(\alpha_d, C_P) = (1.0, 0.0)$ for sustained forces and $(\alpha_d, C_P) = (1.0, 1.38)$ for impulsive forces were set, both types of observed forces were reproduced most accurately. We have found that sustained forces acting on the coastal cliff can be expressed by buoyancy. Thus, it is likely that the cliff boulder starts to move while impulsive forces act on it rather than when sustained forces do. Sustained forces can also be reproduced using $(\alpha_d, C_P) = (1.0, 1.38)$ or $(\alpha_d, C_P) = (1.0 + 0.5F_r^2, 0.0)$, because the velocity when sustained force is generated is rather small. The values $(\alpha_d, C_P) = (1.0, 1.38)$ can reproduce most accurately both impulsive forces and sustained forces.

Using the method proposed in this study, wave forces acting on the notch at the coastal cliff can be estimated from only water depth and velocity. Therefore, the proposed method can be widely applied to understand the size of past extreme waves using only coastal boulder parameters. However, as the impact of scaling on simulating impulsive forces is significant, impulsive forces over coastal cliffs should be

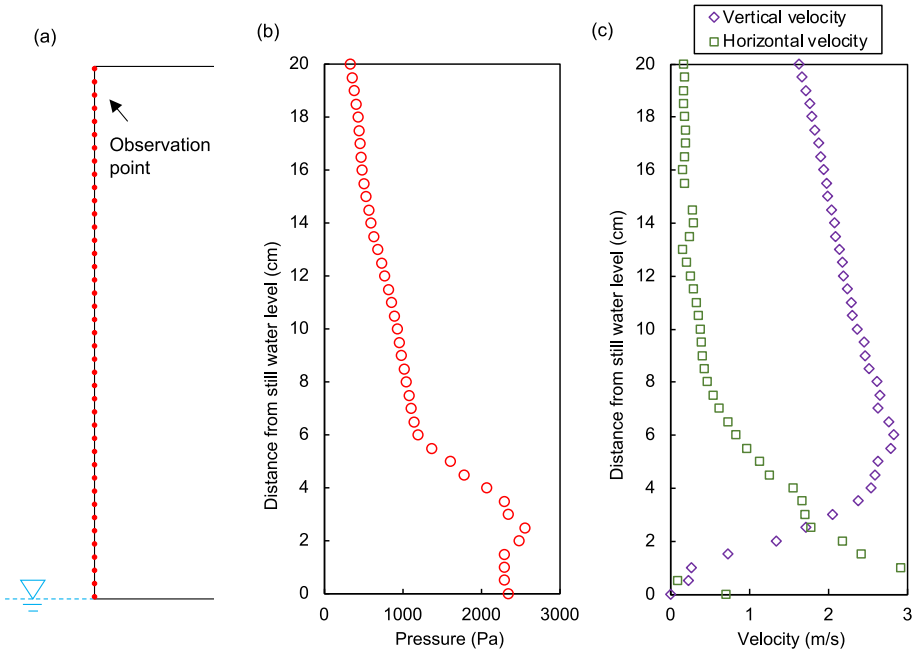

Fig. 14. (a) Observation points at the vertical wall of forces in the numerical simulation using the CADMAS/SURF/3D-2F. (b) The vertical distribution of maximum pressures and (c) horizontal and vertical velocities during the numerical calculation for the vertical wall when the generated wave height was 10 cm.

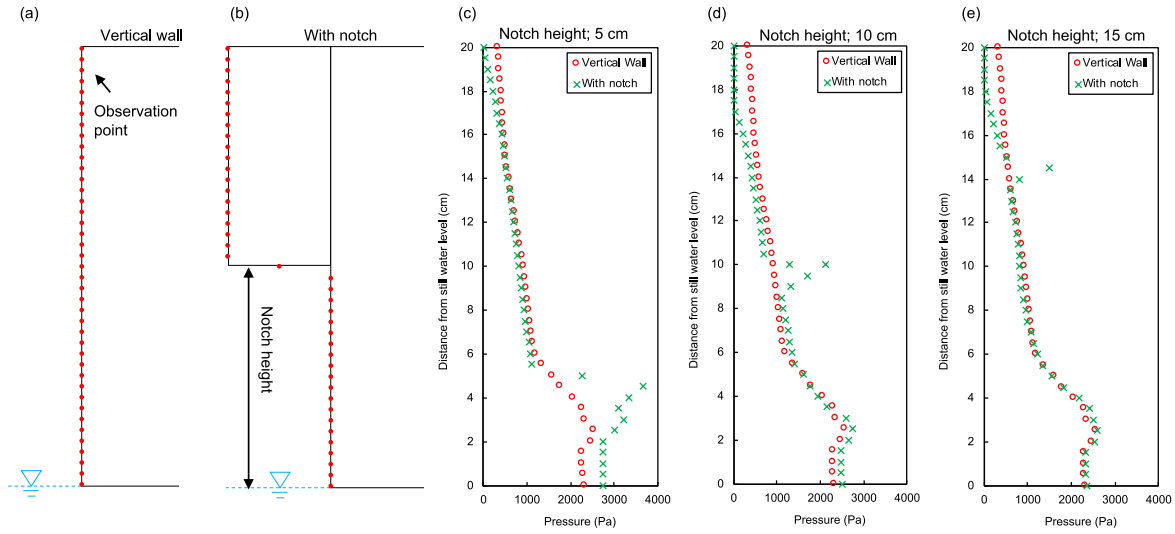

Fig. 15. Observation points of forces in the numerical simulation using the CADMAS/SURF/3D-2F for (a) the vertical wall and (b) the cliff topography with a notch. The vertical distribution of maximum pressures during the numerical calculation for the vertical wall and cliff topography with a notch when the generated wave height was (c) 5 cm, (d) 10 cm, and (e) 15 cm when the generated wave height was 10 cm.

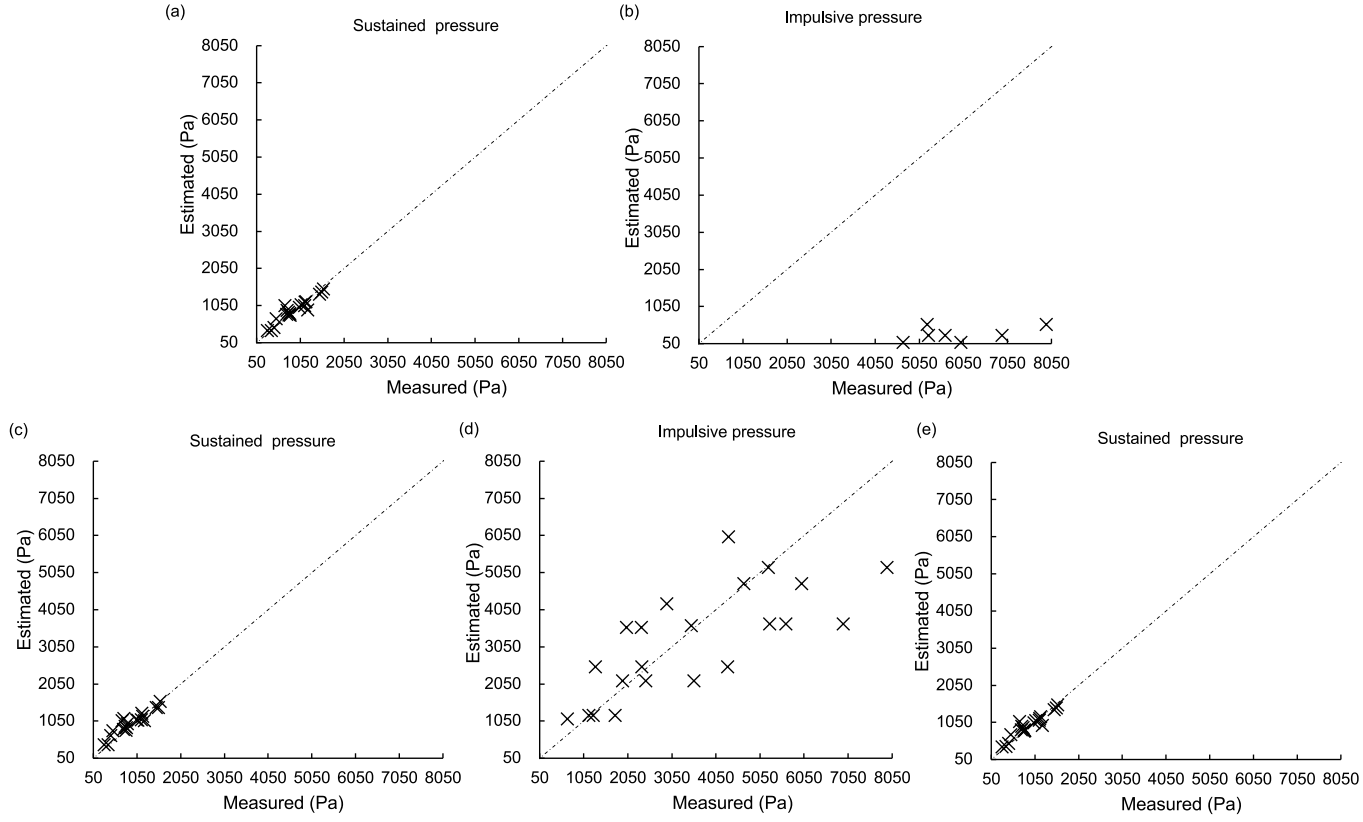

Fig. 16. The measured versus estimated (a) sustained and (b) impulsive force when (α_d, C_P) = (1.0, 0.0). The measured versus estimated (c) sustained and (d) impulsive force when (α_d, C_P) = (1.0, 1.38). (e) The measured sustained forces versus estimated ones using the relation of α_d and F_r shown in equation (9).

investigated at lower scales in the future.

Credit author statement

Masashi Watanabe: Conceptualization, Methodology, Software, Validation, Formal analysis, Investigation, Resources, Data curation, Writing – original draft, Writing – review & editing, Visualization, Supervision, Project administration, Funding acquisition, **Taro Arikawa**: Conceptualization, Methodology, Software, Validation, Formal analysis, Investigation, Resources, Data curation, Writing – review & editing, Visualization, Supervision, Project administration, Funding acquisition.

Table 3
K and κ values versus α_d and C_P values for impulsive wave forces and sustained wave forces.

(α_d, C_P)	K (Impulsive)	κ (Impulsive)	K (Sustained)	κ (Sustained)
(1.0, 0.0)	0.015	3.0	1.06	0.76
(3.0, 0.0)	0.022	4.32	3.17	0.76
(1.0, 1.38)	1.0	1.31	1.14	0.79
($1.0 + 0.5Fr^2$, 0.0)	–	–	1.17	0.72

Declaration of competing interest

The authors declare the following financial interests/personal relationships which may be considered as potential competing interests: Masashi Watanabe reports financial support was provided by Japan Society for the Promotion of Science. Masashi Watanabe reports financial support was provided by the Fukada Geological Institute.

Data availability

No data was used for the research described in the article.

Acknowledgments

This work was supported by a Fukada Grant-in-Aid FY2020 from the Fukada Geological Institute to Masashi Watanabe and JSPS KAKENHI Grant Number 21H00631, 22K14455. This work was also supported by a Sasakawa Scientific Research Grant from the Japan Science Society. This work was also supported by Association for disaster prevention research. This research was also supported by the Earth Observatory of Singapore via its funding from the National Research Foundation Singapore and the Singapore Ministry of Education under the Research Centres of Excellence initiative. This work comprises EOS contribution number 505. We appreciate K. Hiraishi, Y. Enomoto, T. Goto, D. Okamoto, H. Imai and M. Yoshida for their support during laboratory experiment. Simulations were performed on the Earth Simulator at the Japan Agency for Marine–Earth Science and Technology. We greatly appreciate Dr. Pavel Adamek of Nanyang Technological University for the proofreading of the English in the text. We also thank three anonymous reviewers for their valuable suggestions and comments.

References

Aida, I., 1978. Reliability of tsunami source model derived from fault parameters. J. Phys. Earth 26, 57–73.
Arikawa, T., 2015. Consideration of characteristics of pressure on seawall by solitary waves based on hydraulic experiments. Coastal Engineering, Japan Society of Civil Engineers 71 (2), I 889–I 894 (in Japanese).
Arikawa, T., Yamada, H., Akiyama, M., 2005. Study of applicability of tsunami wave force in a three-dimensional numerical wave flume. Japan Society of Civil Engineers Coast. Eng. 52, 46–50 (in Japanese).
Arikawa, T., Ohtubo, D., Nakano, F., Shimosako, K., Takahashi, S., Imamura, F., Matsutomi, H., 2006. Large model test on surge front tsunami force. Japan Society of Civil Engineers Coast. Eng. 53, 796–800 (in Japanese).
Arikawa, T., Takahashi, K., Suzuki, K., Kihara, N., Okamoto, D., Mitsui, J., 2021. Applicability of the numerical simulation of the impulsive wave pressure of solitary waves, 2021 J. Disaster Res. 16 (8), 1286–1297.
Arimitsu, T., Kawasaki, K., 2016. Development of estimation method of tsunami wave pressure exerting on land structure using depth-integrated flow model. Coast Eng. J. 58 (4), 1640021.
Asakura, R., Iwase, K., Ikeya, T., Takao, M., Kaneto, T., Fujii, N., Ohmori, M., 2000. An experimental study on wave force acting on on-shore structure due to overflowing tsunamis. Japan Society of Civil Engineers Coast. Eng. 46, 911–915 (in Japanese).
Asakura, R., Iwase, K., Ikeya, T., Takao, M., Kaneto, T., Fujii, N., Ohmori, M., 2002. The tsunami wave force acting on land structures. Proc. Int. Coast. Eng. Conf. (ICCE2002), ASCE 28, 1191–1202.
Autret, R., Dodet, G., Fichaut, Z.B., Suanez, S., David, L., Leckler, F., Ardhuin, F., Ammann, J., Grandjean, P., Allemand, P., Filipot, J., 2016. A comprehensive hydro-geomorphic study of cliff-top storm deposits on Banneg Island during winter 2013-2014. Mar. Geol. 382, 37–55.
Carbone, F., Dutykh, D., Dudley, J.M., Dias, F., 2013. Extreme wave runup on a vertical cliff. Geophys. Res. Lett. 40, 3138–3143.
Costa, P.J.M., Andrade, C., Freitas, M.C., Oliveira, M.A., da Silva, C.M., Omira, R., Taborda, R., Baptista, M.A., Dawson, A.G., 2011. Boulder deposition during major tsunami events. Earth Surf. Process. Landforms 36, 2054–2068.
Cox, R., 2019. Very large boulders were moved by storm waves on the west coast of Ireland in winter 2013–2014. Mar. Geol. 412, 217–219.
Cox, R., Zentner, D.B., Kirchner, B.J., Cook, M.S., 2012. Boulder ridges on the aran islands (Ireland): recent movements caused by storm waves, not tsunamis. J. Geol. 120 (3), 249–272.
Cross, R.H., 1967. Tsunami surge forces. J. Waterw. Harb. Div. 93 (4), 201–234.
Erdmann, W., Kelletat, D., Scheffers, A., 2018. Boulder transport by storms– Extreme-waves in the coastal zone of the Irish west coast. Mar. Geol. 399 (1), 1–13.
Fichaut, B., Suanez, S., 2011. Quarrying, transport and deposition of cliffTop storm deposits during extreme events: banneg Island, Brittany. Mar. Geol. 283 (1–4), 36–55.
Fukui, Y., Nakamura, M., Shiraishi, H., Sasaki, Y., 1963. Hydraulic study on tsunami. Japan Society of Civil Engineers Coast. Eng. 6, 67–82 (in Japanese).
Gandhi, D., Chavare, K.A., Prizomwala, S.P., Bhatt, N., Bhatt, N.Y., Mohan, K., Rastogi, B. K., 2017. Testing the numerical models for boulder transport through high energy marine wave event: an example from southern Saurashtra, western India. Quat. Int. 444, 209–216.
Goto, K., Kawana, T., Imamura, F., 2010. Historical and geological evidence of boulders deposited by tsunamis, southern Ryukyu Islands, Japan. Earth Sci. Rev. 102 (1–2), 77–99.
Goto, K., Miyagi, K., Kawana, T., Takahashi, J., Imamura, F., 2011. Emplacement and movement of boulders by known storm waves - field evidence from the Okinawa Islands, Japan. Mar. Geol. 283 (1–4), 66–78.
Hall, A.M., 2011. Storm wave currents, boulder movement and shore platform development: a case study from East Lothian, Scotland. Mar. Geol. 243 (1–4), 98–105.
Hall, A.M., Hansom, J.D., Williams, D.M., Jarvis, J., 2006. Distribution, geomorphology and lithofacies of cliff-top storm deposits: examples from the high-energy coasts of Scotland and Ireland. Mar. Geol. 232 (2), 131–155.
Hall, A.M., Hansom, J.D., Jarvis, J., 2008. Patterns and rates of erosion produced by high energy wave processes on hard rock headlands: the Grind of the Navir, Shetland, Scotland. Mar. Geol. 248 (1–2), 28–46.
Hansom, J.D., Barltrop, N.D.P., Hall, A.M., 2008. Modelling the processes of cliff-top erosion and deposition under extreme storm waves. Mar. Geol. 253 (1–2), 36–50.
Herterich, J.G., Cox, R., Dias, F., 2018. How does wave impact generate large boulders? Modelling hydraulic fracture of cliffs and shore platforms. Mar. Geol. 399 (1), 34–46.
Hirt, C.W., Nichols, B.D., 1981. Volume of fluid (VOF) method for the dynamics of free boundaries. J. Comput. Phys. 39 (1), 201–225.
Japan Agency for Marine-Earth Science and Technology (JAMSTEC), undated. Earth Simulator. Available at. http://www.jamstec.go.jp/es/en/system/index.html, Accessed date: 9 November 2021.
Kato, F., Suwa, Y., Fujita, K., Kishida, H., Igarashi, T., Okamura, J., Hayashi, Y., 2012. A method to estimate tsunami setup in front of buildings. Japan Society of Civil Engineers Coast. Eng. 68 (2), I 331–I 335 (in Japanese).
Kennedy, A.B., Mori, N., Yasuda, T., Shimozono, T., Tomiczek, T., Donahue, A., Shimura, T., Imai, Y., 2017. Extreme block and boulder transport along a cliffed coastline (calicoan Island, Philippines) during super typhoon haiyan. Mar. Geol. 383, 65–77.
Kennedy, A.B., Cox, R., Dias, F., 2021. Storm waves may be the source of some "tsunami" coastal boulder deposits. Geophys. Res. Lett. 48, e2020GL090775.
Kihara, N., Niida, Y., Takabatake, D., Kaida, H., Shibayama, A., Miyagawa, Y., 2015. Large-scale experiments on tsunami-induced pressure on a vertical tide wall. Coast. Eng. 99, 46–63.
Kihara, N., Arikawa, T., Asai, T., Hasebe, M., Ikeyae, T., Inoue, S., Kaida, H., Matsutomi, H., Nakano, Y., Okuda, Y., Okuno, S., Ooie, T., Shigihara, Y., Shoji, G., Tateno, T., Tsurudome, C., Watanabe, M., 2021. A physical model of tsunami inundation and wave pressures for an idealized coastal industrial site. Coast. Eng. 169, 103970.
Kogure, T., Matsukura, Y., 2012. Threshold height of coastal cliffs for collapse due to tsunami: theoretical analysis of the coral limestone cliffs of the Ryukyu Islands, Japan. Mar. Geol. 323–325, 14–23.
Kogure, T., Aoki, H., Maekado, A., Hirose, T., Matsukura, Y., 2006. Effect of the development of notches and tension cracks on instability of limestone coastal cliffs in the Ryukyus, Japan. Geomorphology 80 (3–4), 236–244.
Mastronuzzi, G., Pignatelli, C., Sanso, P., Selleri, G., 2007. Boulder accumulations produced by the 20th of February, 1743 tsunami along the coast of southeastern Salento (Apulia region, Italy). Mar. Geol. 242, 191–205.
Miller, S., Rowe, D.A., Brown, L., Mandal, A., 2014. Wave-emplaced boulders: implications for development of "prime real estate" seafront, North Coast Jamaica. Bull. Eng. Geol. Environ. 73, 109–122.
Nandasena, N.A.K., Tanaka, N., 2013. Boulder transport by high energy: numerical model-fitting experimental observations. Ocean Eng. 57, 163–179.
Noormets, R., Crook, K.A.W., Felton, E.A., 2004. Sedimentology of rocky shorelines: 3. Hydrodynamics of megaclast emplacement and transport on a shore platform, Oahu, Hawaii. Sediment. Geol. 57, 163–179.
Nott, J., 2003. Waves, coastal boulder deposits and the importance of the pre-transport setting. Earth Planet Sci. Lett. 210, 269–276.
Nouri, Y., Nistor, I., Palermo, D., Cornett, A., 2010. Experimental investigation of tsunami impact on free standing structures. Coast Eng. J. 52 (1), 43–70.
Okamoto, D., Okubo, H., Kasahara, H., Watanabe, M., Arikawa, T., 2020. Quantitative examination of lift force acting on pier based on gas-liquid phase flow model. Japan Society of Civil Engineers 76 (2), I 787–I 792 (in Japanese).

Okamoto, D., Okubo, H., Kasahara, H., Nakamura, N., Watanabe, M., Arikawa, T., 2021. Study on pressure reduction effect by uplift forces and aperture ratio on horizontal platform based on gas-liquid phase flow model. Japan Society of Civil Engineers 77 (2), I 727–I 732 (in Japanese).
Palermo, D., Nistor, I., Al-Faesly, T., Cornett, A., 2013. Impact of tsunami forces on structures. J. Tsunami Soc. Int 32 (2), 58–76.
Pignatelli, C., Sanso, P., Mastronuzzi, G., 2009. Evaluation of tsunami flooding using geomorphologic evidence. Mar. Geol. 260, 6–18.
Piscitelli, A., Milella, M., Hippolyte, J.C., Shah-Hosseini, M., Morhange, C., Mastronuzzi, G., 2017. Numerical approach to the study of coastal boulders: the case of Martigues, Marseille, France. part A Quat. Int. 439, 52–64.
Rogers, B.D., Dalrymple, R.A., 2008. SPH modeling of tsunami waves. In: Liu, P.L.-F., Yeh, H., Synolakis, C. (Eds.), Advanced Numerical Models for Simulating Tsunami Waves and Runup, vol. 10. World Scientific, pp. 75–100.
Rovere, A., Casella, E., Harris, D.L., Lorscheid, T., Nandasena, N.A.K., Dyer, B., Sandstrom, M.R., Stocchi, P., D'Andrea, W.J., Raymo, M.E., 2017. Giant boulders and last interglacial storm intensity in the north atlantic. Proc. Natl. Acad. Sci. USA 114 (46), 12144–12149.
Sakakiyama, T., 2012. Tsunami inundation flow and tsunami pressure on structures. Japan Society of Civil Engineers Coast. Eng. 68 (2), I 771–I 775 (in Japanese).
Sarfaraz, M., Pak, A., 2017. SPH numerical simulation of tsunami wave forces impinged on bridge superstructures. Coast. Eng. 121, 145–157.
Shimosako, K., 2001. Hydraulic model experiment. Concrete Journal 39 (9), 134–137 (in Japanese).
Shimosako, K., Ohki, Y., Takano, T., Tsuda, M., 2001. Large-scale hydraulic model experiments on impulsive wave forces acting on RC beams and the response characteristics of the members. Japan Society of Civil Engineers Coast. Eng. 48, 836–840 (in Japanese).
Spiske, M., Borocz, Z., Bahlburg, H., 2008. The role of porosity in discriminating between tsunami and hurricane emplacement of boulders - a case study from the Lesser Antilles, Southern Caribbean. Earth Planet Sci. Lett. 268, 384–396.
Steer, J.N., Kimmoun, O., Dias, F., 2021. Breaking-wave induced pressure and acceleration on a clifftop boulder. J. Fluid Mech. 929.
Suanez, S., Fichaut, B., Magne, R., 2009. Cliff-top storm deposits on banneg Island, brittany, France: effects of giant waves in the eastern atlantic ocean. Sediment. Geol. 220 (1–2), 12–28.
Watanabe, M., Goto, K., Imamura, F., Kennedy, A., Sugawara, D., Nakamura, N., Tonosaki, T., 2019. Modeling boulder transport by coastal waves on cliff topography: case study at Hachijo Island, Japan. Earth Surf. Process. Landforms 44 (15), 2939–2956.
Watanabe, M., Kihara, N., Arikawa, T., Tsurudome, C., Hosaka, K., Kimura, T., Hashimoto, T., Ishihara, F., Shikata, R., Morikawa, D.S., Makino, T., Asai, M., Chida, Y., Ohnishi, Y., Marras, S., Mukherjee, A., Cajas, J.C., Houzeaux, G., Paolo, B. D., Lara, J.L., Barajas, G., Losada, Í.L., Hasebe, M., Shigihara, Y., Asai, T., Ikeya, T., Inoue, S., Matsutomi, H., Nakano, Y., Okuda, Y., Okuno, S., Ooie, T., Shoji, G., Tateno, T., 2022. Validation of tsunami numerical simulation models for an idealized coastal industrial site. Coast Eng. J. 64 (2), 302–343.
Whelan, F., Kelletat, D., 2005. Boulder deposits on the Southern Spanish Atlantic coast: possible evidence for the 1755 AD Lisbon tsunami. Sci. Tsunami Hazards 23, 25–38.
Williams, D.M., Hall, A.M., 2004. Cliff-top megaclast deposits of Ireland, a record of extreme waves in the North Atlantic - storms or tsunamis? Mar. Geol. 206, 101–117.